Bump and Trench Modifications to Film-Cooling Holes at the Vane-Endwall Junction

N. Sundaram
Mechanical Engineering Department,
Virginia Polytechnic Institute
and State University,
Blacksburg, VA 24061
e-mail: nasundar@vt.edu

K. A. Thole
Mechanical and Nuclear Engineering Department,
The Pennsylvania University,
University Park, PA 16802

The endwall of a first-stage vane experiences high heat transfer and low adiabatic effectiveness levels because of high turbine operating temperatures and formation of leading edge vortices. These vortices lift the coolant off the endwall and pull the hot mainstream gases toward it. The region of focus for this study is the vane-endwall junction region near the stagnation location where cooling is very difficult. Two different film-cooling hole modifications, namely, trenches and bumps, were evaluated to improve the cooling in the leading edge region. This study uses a large-scale turbine vane cascade with a single row of axial film-cooling holes at the leading edge of the vane endwall. Individual hole trenches and row trenches were placed along the complete row of film-cooling holes. Two-dimensional semi-elliptically shaped bumps were also evaluated by placing the bumps upstream and downstream of the film-cooling row. Tests were carried out for different trench depths and bump heights under varying blowing ratios. The results indicated that a row trench placed along the row of film-cooling holes showed a greater enhancement in adiabatic effectiveness levels when compared to individual hole trenches and bumps. All geometries considered produced an overall improvement to adiabatic effectiveness levels. [DOI: 10.1115/1.2812933]

Introduction

A higher demand in power output for modern gas turbines have resulted in an increase in combustor exit temperatures. Higher temperatures in turn have resulted in flatter profiles at the combustor exit [1] warranting the need for sufficient cooling of endwall surfaces. In addition to these flat profiles, the endwall surfaces also experience high heat transfer due to the formation of leading edge vortices, which tend to lift the coolant off the surface. Friedrichs et al. [2–4] showed that the leading edge on the endwall is the most difficult region to cool. Studies by Thole and Knost [5] showed that even with an upstream leakage flow, the leading edge-endwall junction around the stagnation region remains uncooled.

To achieve higher adiabatic effectiveness levels at the leading edge, it is important to ensure that there is a uniform spread of coolant exiting the film-cooling holes. Typical film-cooling hole designs on a surface give low adiabatic effectiveness levels near and in between the hole exits causing localized regions of hot spots. This study focuses on eliminating these hot spots by improving the adiabatic effectiveness levels at the leading edge region of a vane endwall.

Since effective cooling at the leading edge is a challenge to a turbine designer, new cooling methods are desired. This study is aimed at understanding the effect of modifying the coolant jet trajectory at the cooling hole exit and how it enhances the adiabatic effectiveness levels. The work presented in this paper compares the effect of two different modifications on the adiabatic effectiveness levels at the leading edge, namely, trenches and bumps.

Relevant Past Studies

Effective cooling of a turbine surface is highly important for its improved operational life and the performance of the engine as a whole. With regard to that, a number of studies have focused on developing alternate methods to cool a surface in addition to placing film-cooling holes.

An early study was carried out by Blair [6] in which he showed that coolant flow from an upstream slot resulted in higher cooling near the suction side and reduced cooling near the pressure side. This nonuniform cooling was as a result of the coolant being swept from the pressure side to the suction side caused by the secondary flow within the vane passage. Knost and Thole [7] studied the effect of leakage flow through the combustor-vane interface onto the endwall adiabatic effectiveness levels. Similar to Blair [6], they also showed that the coolant exits the upstream slot in a nonuniform fashion. The nonuniformity was associated with the formation of a hot ring around the stagnation region toward the pressure side of the vane. Cardwell et al. [8] showed that the size of this hot ring can be reduced by decreasing the width of the upstream slot, which results in a more uniform spread of coolant. Burd and Simon [9] studied the effects of slot bleed injection over the contoured endwall of a nozzle guide vane. They concluded from their measurements that bleed cooling from upstream of the leading edge of the vane provides considerable thermal protection within the passage. These studies of coolant flow through a slot showed that effective cooling can be achieved by injecting a 2D layer of film cooling over the surface.

Searching for better cooling techniques, Bunker [10] measured improved film-cooling effectiveness levels on a flat plate using discrete holes placed within a transverse slot with varying widths. Bunker [10] showed that the narrowest possible slot width relative to the interior cooling hole diameter is most desirable. As placing cooling holes in slots basically modifies the hole exit, there have been few studies that have investigated this particular effect. Lu et al. [11] investigated the effect of slot exit area and edge shape on film effectiveness measurements made on a flat plate. They found that a straight edge exit performed the best at a blowing ratio of $M=1.0$, whereas a ramped exit enhanced the adiabatic effectiveness levels at lower blowing ratios. Waye and Bogard [12] applied the trench configuration on the suction side of a first-stage vane with varying slot exit configurations. They tested a narrow trench where the trench wall was at the film-cooling hole exit, a wide trench where the trench wall was at a distance of one cooling hole

Contributed by the International Gas Turbine Institute of ASME for publication in the JOURNAL OF TURBOMACHINERY. Manuscript received June 6, 2007; final manuscript received June 26, 2007; published online August 1, 2008. Review conducted by David Wisler. Paper presented at the ASME Turbo Expo 2007: Land, Sea and Air (GT2007), Montreal, Quebec, Canada, May 14–17, 2007.

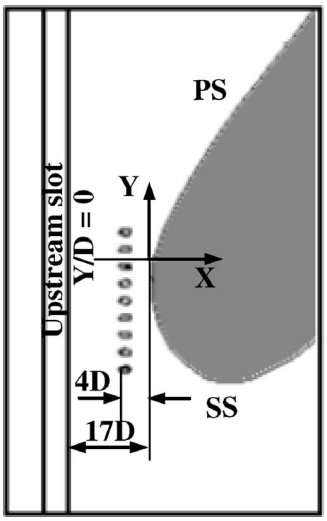

Fig. 1 Illustrates the endwall design studied at the leading edge

diameter from the hole exit, and a trench with an angled exit. They also found that the narrow trench performed the best relative to a wide trench and angled exit trench and the adiabatic effectiveness levels peaked for blowing ratios beyond $M=1.0$.

A recent study was carried out by Sundaram and Thole [13] to understand the effect of placing semi-elliptically shaped deposits downstream of a row of cooling holes. While their study was aimed at understanding how deposits could adversely affect cooling levels, their results indicated improved cooling performance for some geometries. They carried out this study at the leading edge of a first-stage vane endwall on a rough surface and found that smaller deposits enhanced adiabatic effectiveness levels. As the deposit height was increased, the effectiveness levels were reduced below that of the baseline with no bumps.

In summary, different modifications have been applied to film-cooling holes to enhance the adiabatic effectiveness levels. Most of these studies have been on a flat plate with no studies carried out at the leading edge of a first-stage vane endwall with the exception of the authors' previous work [13].

Bump and Trench Descriptions

Previous studies by Bunker [10] and Waye and Bogard [12] showed that holes in a slot are effective in forming a layer of protective film over the surface. These studies also showed that the edges of the slot were very close to the exit of the film-cooling hole for enhanced cooling. The effect of placing cooling holes in a trench was found to show a significant enhancement in effectiveness levels. The trench on the surface can be manufactured during the thermal barrier coating (TBC) application process [14] and its effect can differ with varying trench depths as the thickness of the TBC can be varied. Similarly, studies by Sundaram and Thole [13] also showed that when the edges of the semi-elliptical deposits (bumps) were close to the cooling hole exit, the cooling effectiveness levels were enhanced.

Motivated from these studies, modifications were applied to the leading edge region of the first-stage vane endwall, as shown in Fig. 1. The endwall of the vane was constructed of foam because of its low thermal conductivity (0.033 W/m K). The endwall surface was covered with a thin layer of Balsa wood to simulate a smooth TBC. All of the different configurations were tested on a smooth endwall surface. The endwall leading edge consisted of a single row of axial film-cooling holes with a hole spacing corresponding to $P/D=3$. The cooling row was placed four cooling hole diameters ($4D$) upstream from the stagnation location. An upstream slot, representing the combustor-turbine gap, was placed

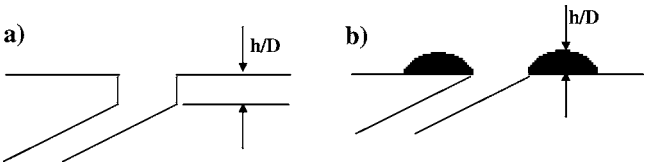

Fig. 2 Illustrates the (*a*) trench geometry and (*b*) bump geometry studied at the leading edge

$17D$ from the stagnation location. Note that it is important to simulate the upstream slot since this interface exists in most turbines and the exiting slot flow influences the upstream boundary condition. Figures 2(a) and 2(b) show the geometries of the two modifications studied at this leading edge location. Figure 2(a) illustrates the trench geometry and Fig. 2(b) illustrates the bump geometry previously described by Sundaram and Thole [13]. For the trench configuration, three different depths were studied corresponding to $h/D=0.4$, 0.8, and 1.2. The trench depths were controlled by varying the thickness of the Balsa wood covering the endwall surface. Three different bump heights were also tested at the leading edge. Similar to Sundaram and Thole [13], these heights corresponded to $h/D=0.5$, 0.8, and 1.2.

Based on the above two concepts, four different cooling hole configurations were tested at varying blowing ratios, as shown in Figs. 3(a)–3(d). Figure 3(a) illustrates the baseline case, which simulated a smooth endwall without any surface modifications. It consisted of a row of axial film-cooling holes placed 30 deg to the endwall surface. Figure 3(b) simulates the individual hole trench configuration, where the trench surrounded each individual cooling hole. Figure 3(c) is the row trench configuration, similar to the one tested by Bunker [10] on a flat plate, where the trench runs along the entire length of the cooling row. Bunker [10] studied only a single trench depth of $h/D=0.43$ for the axial hole geometry. Figure 3(d) is the bump configuration, in which two semi-elliptical bumps were placed at the upstream and downstream locations of the film-cooling hole. The geometries shown in Figs. 3(b)–3(d) will be compared with the baseline case to see if these modifications result in any enhancement.

Experimental Methodology

The experimental section was placed in a closed loop wind tunnel facility, as shown in Fig. 4. The flow encounters an elbow downstream of the fan and passes through a primary heat exchanger used to cool the bulk flow. The flow is then divided into three channels including the center passage and two cooled secondary passages located above and below the test section. Note that only the top secondary passage was used for this study. The primary core flow, located in the center passage, convects through a heater bank where the air temperature is increased to about 60°C. The secondary flow, in the outer passage, was cooled to about 20°C, thereby maintaining a temperature difference of 40°C between the primary and secondary flows. The secondary flow provided the coolant through the film-cooling holes and through the upstream slot. Also, for all the tests carried out in this study, a density ratio of 1.1 was maintained between the coolant

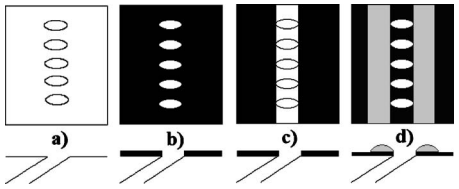

Fig. 3 Schematic of the four configurations: (*a*) baseline, (*b*) individual trench, (*c*) row trench, and (*d*) bumps tested at the leading edge

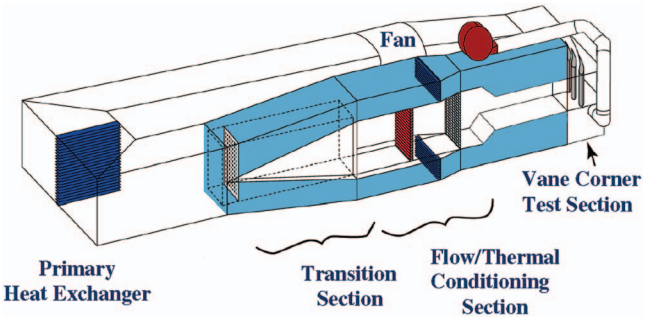

Fig. 4 Illustration of the wind tunnel facility

and mainstream flows. As the density ratios are not being matched to that of the engine, velocity ratios for the cooling holes will be significantly higher than those found in an engine for the same mass flux or momentum flux ratios. While there have been studies indicating that momentum flux scales jet lift-off for flat plate film cooling, it is unknown as to whether it best scales lift-off for endwall film cooling.

Downstream of the flow/thermal conditioning section is the test section that consists of two full passages with one center vane and two half vanes. Table 1 provides a description of the turbine vane geometry and operating conditions. Table 1 also gives the inlet boundary layer characteristics. The boundary layer approaching the vane cascade was measured at $0.63C$ upstream of the vane stagnation. The measurement was done far upstream from the stagnation as the upstream slot flow influences the boundary layer approaching the vane cascade. The vane geometry used in the current study is a commercial first-stage vane previously described by Radomsky and Thole [15]. The passage under study consisted of an endwall surface with film-cooling holes and leakage paths simulating the combustor-vane interface (upstream slot) and vane-to-vane interface. A detailed description of the endwall construction has been previously described by Knost and Thole [5].

The inlet turbulence intensity and length scales were measured to be 1.3% and 4 cm, respectively. These tests were carried out at a low turbulence intensity of 1.3% to isolate the effects of trenches and bumps on endwall adiabatic effectiveness levels. For every test condition, the dimensionless pressure coefficient distribution was verified to ensure periodic flow through the passages. Two separate plenums were used to control the coolant flowrate through the upstream slot and through the film-cooling holes, respectively. The upstream slot flow was assumed to have a discharge coefficient of 0.6, which is the assumed value for a flow through a sharp-edged orifice, and the blowing ratio was calculated accordingly. The coolant flowrate through the film-cooling holes was set based on an average ideal blowing ratio. This blowing ratio was based on an inviscid calculation through the holes and the inlet mainstream velocity. It should be noted that an average discharge coefficient was not assumed to set the coolant flow through the film-cooling holes as it varies from hole to hole.

Table 1 Geometric and flow conditions

Scaling factor	9
Scaled up chord length (C)	59.4 cm
Pitch/chord (P/C)	0.77
Span/chord (S/C)	0.93
Hole diameter (D)	0.46 cm
Hole L/D	8.3
Re_{in}	2.1×10^5
Inlet and exit angles	0 deg and 72 deg
Inlet and exit Mach numbers	0.017 and 0.085
Inlet mainstream velocity	63 m/s
Boundary layer thickness/span (δ/S)	0.18
Displacement thickness/span (δ^*/S)	0.025
Momentum thickness/span (θ/S)	0.020
Upstream slot width	$0.024C$

Instrumentation and Temperature Measurements. A FLIR P20 infrared camera was used to spatially resolve adiabatic wall temperatures on the endwall. Measurements were taken at six different viewing locations to ensure that the entire endwall surface was mapped. The camera was placed perpendicular to the endwall surface at a distance 55 cm from the endwall. Each picture covered an area 24×18 cm^2 with the area being divided into 320 $\times240$ pixel locations. The spatial integration of the camera was 0.715 mm (0.16 hole diameters). Thermocouples were also placed on the endwall surface at different locations to directly measure the temperature to postcalibrate the infrared images. For the postcalibration, the emissivity was set at a constant value of 0.92 and the background temperature ($\sim45^\circ$C) was adjusted until the temperatures from the infrared camera images were within 0.05°C of the corresponding thermocouple data. Six images were taken at each of the viewing locations to obtain an averaged picture using an in-house MATLAB program. The same program was also used to assemble the averaged pictures at all locations to give a complete temperature distribution along the passage endwall.

Freestream temperatures were measured at multiple locations along the pitch and the average was determined by using a thermocouple rake consisting of three thermocouples along the span. It was found that the variations along the pitch were less than 0.2°C and that along the span were less than 1.5°C. Voltage outputs from the thermocouples were acquired by a 32 channel data acquisition module that was used with a 12 bit digitizing card. The temperature data were compiled after the system reached steady state.

A 1D conduction correction as described by Ethridge et al. [16] was applied to all adiabatic effectiveness measurements to account for conduction losses through the endwall surface. The conduction correction was applied by measuring the endwall surface effectiveness with no blowing through the film-cooling holes. This was done by blocking the film-cooling holes on the endwall passage under study while maintaining similar flowrates through the adjacent passage to ensure the correct boundary condition under the endwall. At the entrance to the flow passage for a measured value of $\eta=0.9$, a correction of 0.16 was typical while along the pressure side for a measured value of $\eta=0.1$, a correction of 0.03 was applied.

Experimental Uncertainty. An uncertainty analysis was performed on the measurements of adiabatic effectiveness and blowing ratio using the partial derivative method described at length by Moffat [17].

For adiabatic effectiveness measurements, the precision uncertainty was determined by taking the standard deviation of six measurement sets of IR camera images with each set consisting of six images. The precision uncertainty of the measurements was $\pm0.014^\circ$C. The bias uncertainty was $\pm1.0^\circ$C based on the uncertainty in the IR camera measurements specified by the manufacturer. The bias uncertainty of the thermocouples was $\pm0.5^\circ$C as specified by the manufacturer and the bias uncertainty associated with the digitizing card was $\pm0.35^\circ$C. Then, the total bias uncertainty of the temperature measurement due to the thermocouple and the digitizing card was calculated to be $\pm0.61^\circ$C. The total uncertainty was then calculated as $\pm1.02^\circ$C for the images and $\pm0.62^\circ$C for the thermocouple measurements. Uncertainty in effectiveness η was found based on the partial derivative of η with respect to each temperature in the definition and the total uncertainty in the measurements. Uncertainties in adiabatic effectiveness were calculated to be $\partial\eta=\pm0.032$ at a η value of 0.2 and $\partial\eta=\pm0.033$ at a η value of 0.9.

To calculate the uncertainty in blowing ratio, the uncertainties associated with the pressure transducers, the Pitot probe, and the

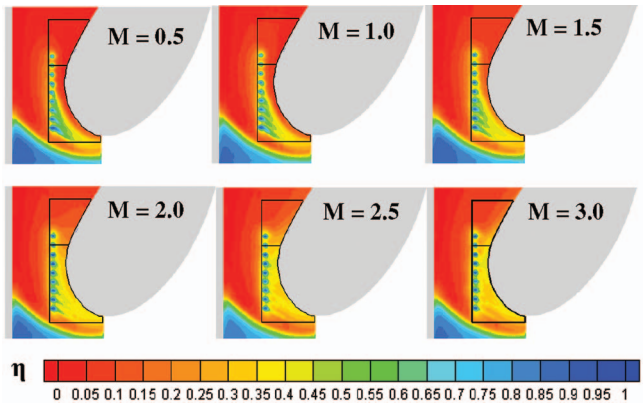

Fig. 5 Contours of adiabatic effectiveness comparing the baseline case at different blowing ratios

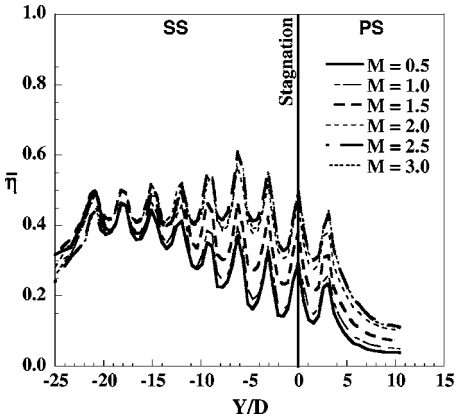

Fig. 6 Lateral average effectiveness plots of the baseline case

thermocouples were taken into account. The pressure transducer had a total uncertainty of ± 0.13 Pa and the pitot probe which was used to measure the inlet mainstream velocity had a total uncertainty of ± 0.22 Pa. The total uncertainty of the thermocouples as explained earlier was $\pm 0.62°C$. The uncertainties in blowing ratio were then calculated to be $\partial M = \pm 0.045$ at a value of $M = 0.5$ and $\partial M = \pm 0.052$ at a value of $M = 3.0$.

Discussion of Results

As mentioned previously, the baseline case was measured on a smooth endwall surface. baseline tests were carried out at six film-cooling blowing ratios varying from $M = 0.5$ to $M = 3.0$, as shown in Fig. 5. A flowrate corresponding to an inlet blowing ratio of $M_{in} = 0.3$ was set through the upstream slot for all the tests.

It can be seen from the contours in Fig. 5 that at low blowing ratios, the adiabatic effectiveness levels are higher on the suction side of the endwall than on the pressure side. This is because of the lower static pressure on the suction side, which enables more coolant to exit the cooling holes near the suction side. With an increase in blowing ratio up to $M = 2.0$, there is a gradual increase in effectiveness levels along the pressure and suction sides. A further increase beyond $M = 2.0$ results in an increase in effectiveness levels on the pressure side with subsequent decrease on the suction side when compared to the lower blowing ratio. It can also be seen that at higher blowing ratios, there is a reduction in effectiveness levels just downstream of the cooling holes. At high blowing ratios, the coolant jets are associated with high momentum resulting in jet lift-off from the surface. It is also seen that at these high blowing ratios, the adiabatic effectiveness levels increase near the vane-endwall junction. The adiabatic effectiveness levels also increase because of the horseshoe vortex formed at the leading edge, which pulls the coolant injected into the mainstream flow back to the surface. As a result, the adiabatic effectiveness levels increase at the vane-endwall junction along both the pressure and suction sides.

Figure 6 compares the lateral average effectiveness ($\bar{\eta}$) at varying blowing ratios for the baseline case. Adiabatic effectiveness values were laterally averaged in the streamwise (X direction), direction as shown in Fig. 1. Figure 1 also shows the stagnation location along the pitch where $Y/D = 0$. Lateral averaging was calculated for two areas on either side of the stagnation location; suction side extending from $Y/D = 0$ to $Y/D = -25$ and pressure side extending from $Y/D = 0$ to $Y/D = 10$ (refer to Fig. 5). For calculating the lateral average, the area under consideration was divided into many small divisions starting at different pitch (Y/D) locations. The adiabatic effectiveness values were then averaged along each of these divisions to give the laterally averaged adiabatic effectiveness along the pitch. Note that lateral averaging was carried out for the same vane surface length of $x/S = 0.15$ along the suction and pressure sides from the vane stagnation.

From Fig. 6, it can be seen that for blowing ratios from $M = 0.5$ to $M = 2.0$, the effectiveness levels increase on the suction side until $Y/D = -10$. Any subsequent increase in blowing ratio caused an increase on the pressure side and a decrease on the suction side. It is interesting to note that at a blowing ratio of $M = 2.0$, the effectiveness levels are the highest on the suction side as well on the pressure side when compared to other blowing ratios. The formation of peaks and valleys in the lateral average plot clearly show that at every blowing ratio, there is a variation in adiabatic effectiveness levels between the film-cooling holes. The variation in effectiveness levels is because of the formation of hot spots as a result of nonuniform coolant spread on the endwall surface.

The variation in adiabatic effectiveness levels on the suction and pressure sides can also be studied by comparing their area-averaged effectiveness ($\bar{\bar{\eta}}$). Figure 7 compares the area-averaged effectiveness for the baseline cases at different blowing ratios. An overall area-averaged effectiveness was calculated for the combined (SS+PS) region by averaging the adiabatic effectiveness values extending from the suction side to the pressure side ($Y/D = -25$ to $Y/D = 10$). Note that lateral averaging was carried out for the same vane surface length of $x/S = 0.15$ along the suction and pressure sides from the vane stagnation. The area-averaged effectiveness of the combined region increases until a blowing ratio of $M = 2.0$ and then steadies out with any further increase. By looking at the individual effectiveness levels, on the suction side, it peaks at $M = 2.0$ and then decreases and plateaus,

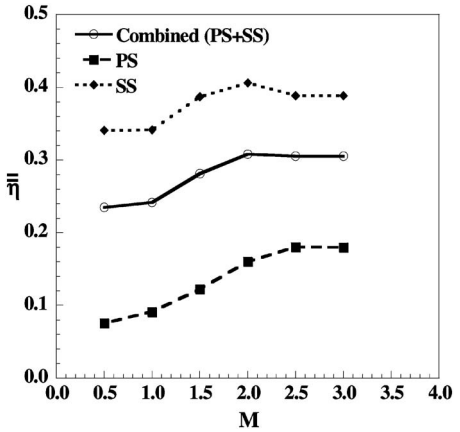

Fig. 7 Area-averaged effectiveness for the baseline geometry along suction, pressure, and the whole leading edge region

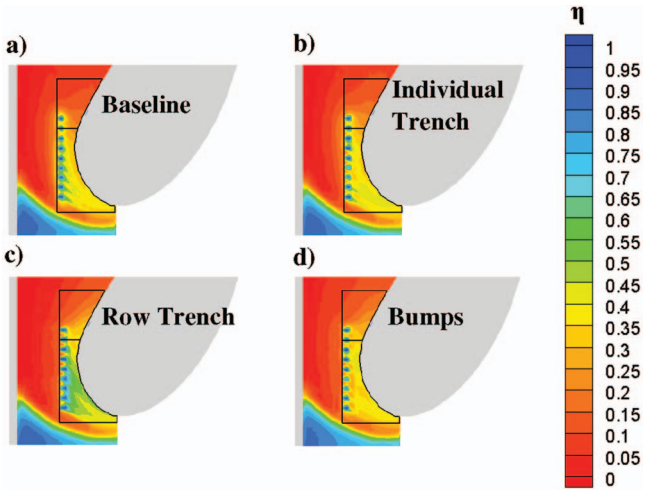

Fig. 8 Contours of adiabatic effectiveness comparing the baseline case with the other configurations at a blowing ratio of $M=2.0$

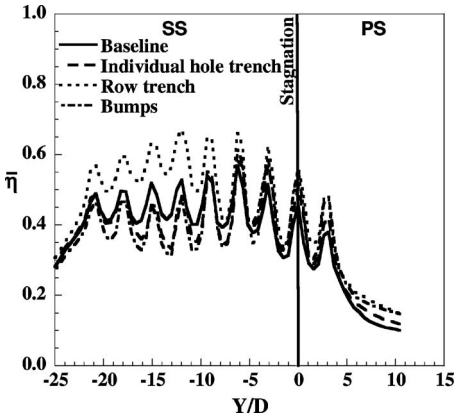

Fig. 9 Laterally averaged adiabatic effectiveness comparing the effect of trenches and bumps at the leading edge at $M=2.0$

whereas on the pressure side, the effectiveness levels keep increasing with an increase in blowing ratio. So, for the baseline case with a smooth endwall surface, a blowing ratio of $M=2.0$ was found to have the highest effectiveness levels.

Effect of Modifying the Film-Cooling Hole Exit. An individual hole trench, a row trench, and a bump configuration upstream and downstream of the cooling row were tested on a smooth endwall surface. These modifications were carried out at a constant coolant flowrate through the upstream slot. It was shown by Thole and Knost [5] that for a two passage study, the coolant flow from the upstream slot is an important characteristic to simulate given that it provides the correct incoming boundary conditions to the vane cascade. Their study showed that due to secondary flows in the vane passage, the coolant flow from the upstream slot was swept from the pressure side to the suction side, creating a low adiabatic effectiveness zone around the stagnation region. They also found that in the presence of leading edge film-cooling holes, the variation in adiabatic effectiveness levels around the stagnation region was solely the result of coolant flow from the film-cooling holes. Hence, it was concluded that the upstream slot did not influence the comparisons with respect to trenches and bumps. Note that for these comparisons, the same pressure ratio was used to set the blowing ratio through the film-cooling holes for the baseline and the trench and bump modifications.

Figures 8(*a*)–8(*d*) compare the contours of adiabatic effectiveness of the three modified film-cooling hole exit configurations with the baseline case at a blowing ratio of $M=2.0$. In this section, the baseline is compared with the smallest trench depth and bump height. The smallest trench depth studied corresponded to $0.4D$ and the smallest bump height corresponded to $0.5D$. Comparing the individual hole trench (Fig. 8(*b*)) at $M=2.0$ to the baseline case (Fig. 8(*a*)), it is seen that due to a presence of a vertical wall at the cooling hole exit, the jets are detached from the surface but reattach further downstream of the holes. Hence, the adiabatic effectiveness levels are lower at the exit of the cooling holes. The row trench in Fig. 8(*c*) showed the maximum enhancement in effectiveness levels on the leading edge. The trench walls upstream and downstream of the holes allow the coolant to spread laterally within the trench area, resulting in enhancements in adiabatic effectiveness levels. It is speculated by Bunker [10] that the trench walls reduce the typical vortex motion of the coolant jets and thereby preventing the hot gases from getting pulled underneath the coolant jets.

Placing bumps on the smooth surface caused varied results. From Fig. 8(*d*), it can be seen that relative to the baseline case, it lowered the effectiveness levels on the suction side, whereas it increased the effectiveness levels on the pressure side. Bumps downstream of the cooling holes deflected the coolant jets off the surface, thereby lowering the adiabatic effectiveness levels on the suction side, but caused an increase in effectiveness on the pressure side.

The effects of these modifications are quantified by calculating the laterally averaged effectiveness downstream of the film-cooling holes. From Fig. 9, it can be seen that row trench performed the best on the suction and pressure sides. The individual hole trench and the bumps showed a reduction in adiabatic effectiveness levels from $Y/D=-25$ to $Y/D=-5$ and showed an improvement in effectiveness levels from $Y/D>-5$. The lateral averaged effectiveness curves for the baseline and individual trench seem to coexist with little variation. Their effects at varying blowing ratios can be seen in Fig. 10, which compares the area-averaged effectiveness for the three modifications. At a blowing ratio of $M=2.0$, the area-averaged adiabatic effectiveness of the trenched hole, bumps, and the baseline coexists, showing that their overall effectiveness levels downstream of the cooling holes are the same. Trenches show an improvement over the whole range of blowing ratios tested with the maximum enhancement at a blowing ratio of $M=2.5$.

This initial study was to ascertain which geometry has the maximum effect on the effectiveness levels at the leading edge. Trenches showed an overall enhancement in effectiveness levels and the bumps showed an improvement along the pressure side.

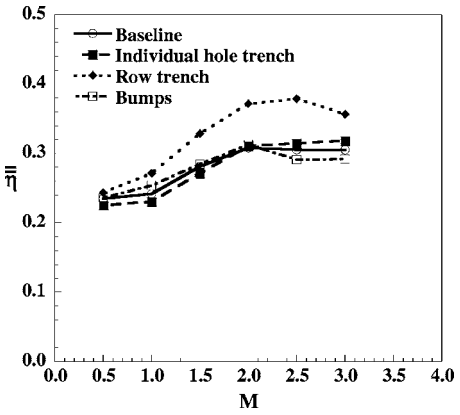

Fig. 10 Area-averaged effectiveness showing the effect of trenches and bumps on film-cooling effectiveness

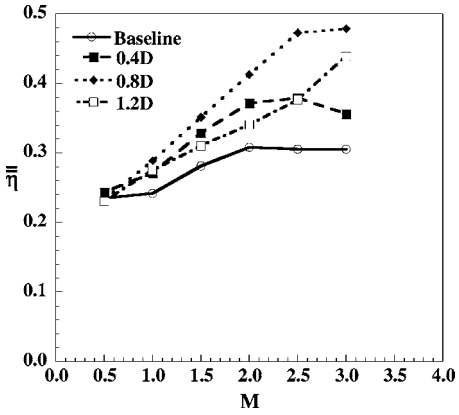

Fig. 11 Area-averaged effectiveness showing the effect of different trench depths for the row trench configuration at varying blowing ratios

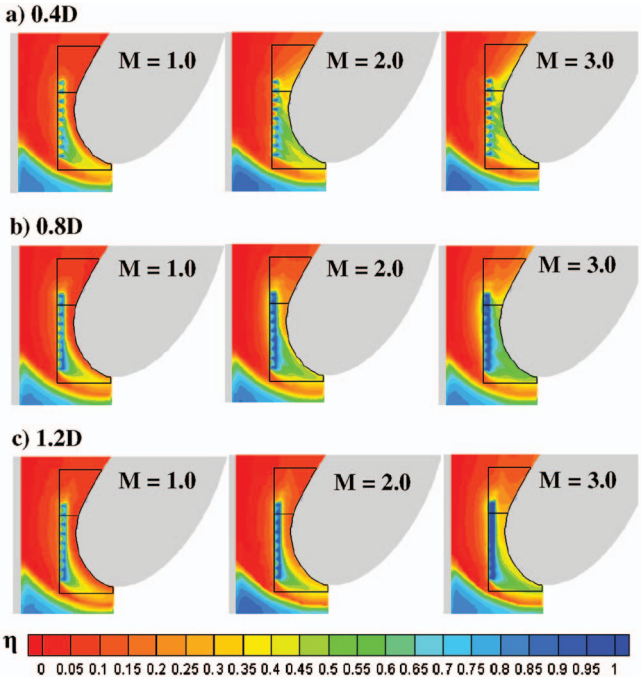

Fig. 12 Contours of adiabatic effectiveness showing the effect of varying the trench depth for the row trench configuration at three different blowing ratios

The sensitivity of varied bump heights and trench depths to blowing ratios will be presented in the following sections.

Effect of Trench Depths on Adiabatic Effectiveness Levels. Three different row trench depths corresponding to 0.4*D*, 0.8*D*, and 1.2*D* were tested on a smooth endwall surface. This study was conducted to investigate the trench depth sensitivity to adiabatic effectiveness levels. Figure 11 compares the area-averaged adiabatic effectiveness of the different trench depths. At the smallest trench depth of 0.4*D*, the enhancements in adiabatic effectiveness levels were seen for all blowing ratios. The adiabatic effectiveness levels for 0.4*D* trench increased with increasing blowing ratio up to a blowing ratio of $M=2.5$. Upon a further increase in blowing ratio to $M=3.0$, the effectiveness levels slightly dropped as a result of higher jet momentum associated with the coolant flow.

As the trench depth was further increased to 0.8*D*, higher enhancements in effectiveness levels were seen for all blowing ratios. Contrary to the 0.4*D* trench, the adiabatic effectiveness for the 0.8*D* trench depth increased until a blowing ratio of $M=2.5$, and then stayed nearly the same with a further increase to $M=3.0$. Compared to the baseline, the enhancement in effectiveness varied from $\eta=0.24$ at $M=1.0$ to a high value of almost $\eta=0.48$ at $M=3.0$.

An increase in trench depth to 1.2*D* also showed enhancements compared to the baseline case but the effectiveness levels were comparatively lower than the 0.8*D* trench, as seen in Fig. 11. Also, the effectiveness levels at 1.2*D* depth were similar or lower than the 0.4*D* depth for blowing ratios less that $M=2.5$ and showed higher levels only at $M=3.0$. At a higher depth and low blowing ratio, the walls of the trench prevent the coolant from exiting uniformly resulting in lower effectiveness levels. As the blowing ratio is increased, the jets exit at a higher momentum making the trench more effective in the spreading of the coolant. From Fig. 11, it can also be seen that the adiabatic effectiveness levels for the 1.2*D* trench follow a different pattern when compared to the 0.4*D* and 0.8*D* trenches.

Figure 12 compares the adiabatic effectiveness levels for three blowing ratios at $M=1.0$, $M=2.0$, and $M=3.0$ for different trench depths. The downstream edge of the trench forms a wall at the film hole exit, which forces the coolant to spread laterally within the trench before convecting over the endwall surface. At a smaller trench depth of 0.4*D*, it is seen that with an increase in blowing ratio, the coolant spreads downstream of the cooling holes in a more uniform manner until the blowing ratio is high enough resulting in jet lift-off. At a high blowing ratio of $M=3.0$, there is less lateral spreading of coolant within the trench resulting in a deterioration in effectiveness levels.

An increase in trench depth to 0.8*D* results in a better lateral spread of coolant within the trench as there is less interaction between the mainstream gases and the coolant than when a set of axial holes are placed on a flat endwall surface. The contours of the 0.8*D* trench show that there are fewer hot spots between the cooling holes when compared to the 0.4*D* trench at the same blowing ratios. It is speculated that with an increase in trench depth, the vortical nature of the flow leaving the cooling holes at the exit is less intense preventing the hot gases from getting pulled down to the surface resulting in a better lateral spread within the trench. Lateral spreading within the trench causes the coolant to exit the trench in a more uniform manner onto the endwall surface. When the trench depth is further increased to 1.2*D*, it is seen that at low blowing ratios, there is an increase in the coolant retention within the trench. A higher depth causes a recirculation of coolant within the trench preventing it from convecting over the surface. With an increase in blowing ratio, the amount of coolant spreading onto the surface increases. As this study was done only until a maximum blowing ratio of $M=3.0$, it is speculated that the 1.2*D* trench will perform better at a blowing ratio of $M=3.0$ or higher.

The uniform spread of coolant as a result of trenches can also be seen by comparing the laterally averaged effectiveness at different blowing ratios for the 0.8*D* trench, as shown in Fig. 13. For the baseline cases (refer to Fig. 6), the laterally averaged adiabatic effectiveness levels showed definite peaks and valleys indicating regions of low effectiveness between the cooling holes. With the trench, it is seen from Fig. 13 that the height between the peaks and valleys is smaller and this height becomes smaller as the blowing ratio is increased, thus indicating a more uniform spread of coolant over the endwall surface. Also, the 0.8*D* trench was found to be the optimum depth from the three trench depths tested, and the performance is highly sensitive to blowing ratio.

Effect of Bump Heights on Adiabatic Effectiveness Levels. Three different bump heights corresponding to 0.5*D*, 0.8*D*, and 1.2*D* were also evaluated at the leading edge on a smooth endwall surface. Figure 14 compares the area-averaged effectiveness for the varying bump heights with the baseline case. The 0.5*D* and

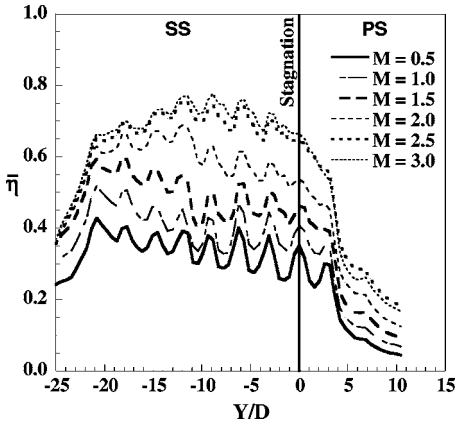

Fig. 13 Lateral averaged effectiveness showing the effect of the 0.8*D* trench depth at different blowing ratios

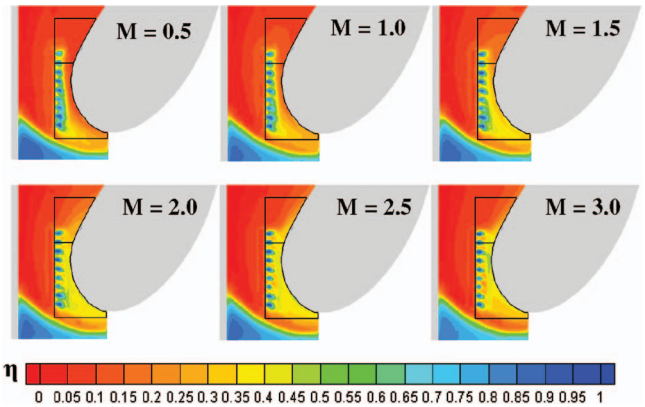

Fig. 15 Contours of adiabatic effectiveness showing the effect of the 1.2*D* bumps at different blowing ratios

0.8*D* bumps showed little effect on modifying the adiabatic effectiveness levels downstream of the film-cooling holes. When the bump height was increased to 1.2*D*, there was an increase in effectiveness levels up to a blowing ratio of $M=2.0$ and a further increase in blowing ratio resulted in lower effectiveness levels.

The variation in effectiveness levels caused by the 1.2*D* bumps can be explained by the adiabatic effectiveness contours shown in Fig. 15. The increase in blowing ratio results in an increase in coolant mass flow rate, which in turn increases the effectiveness levels. At lower blowing ratios of $M=0.5$ and $M=1.0$, the jets are more attached to the surface and they are obstructed by the presence of the bumps. As a result, the coolant accumulates between the cooling holes thereby preventing it from spreading downstream. As the blowing ratio is increased, it can be seen that there is less coolant accumulation between the cooling holes. With the increase in blowing ratio, the coolant injects directly into the mainstream resulting in the formation of hot spots at the exit of the cooling holes. At high blowing ratios, the effectiveness levels further downstream of the cooling holes are higher than at low blowing ratios as a result of jet reattachment. $M=2.0$ was found to be an optimum blowing ratio where there is minimal coolant accumulation between the cooling holes and more spreading downstream of the cooling holes.

The performance of the 1.2*D* bumps along the pressure and suction sides at different blowing ratios can be compared using the laterally averaged effectiveness shown in Fig. 16. Similar to the baseline study, the bumps performed better on the suction side at lower blowing ratio, whereas the effectiveness levels were higher on the pressure side at higher blowing ratios. As mentioned previously, the bumps performed the best at a blowing ratio of $M=2.0$.

Summary of Cooling Enhancements

To summarize the results, Fig. 17 shows the percent increase in area-averaged adiabatic effectiveness levels as a result of placing trenches of different depths at the leading edge. Figure 18 shows the enhancements in adiabatic effectiveness levels as a result of placing bumps of different heights at the leading edge. Trenches showed an enhancement for all depths tested, whereas bumps performed better only at higher heights when compared to the baseline cases.

Trenches typically showed little effect at the lowest blowing ratio of $M=0.5$. For a blowing ratio of $M=1.0$ and higher, the percent enhancements ranged from 10% to almost as high as 60%. The enhancement caused by the 0.8*D* trench was the highest at a blowing ratio of $M=2.5$, beyond which there was a small increase in effectiveness at $M=3.0$. The 1.2*D* trench showed a different trend compared to 0.4*D* and 0.8*D*. The cooling enhancement of the 1.2*D* trench was similar up to a blowing ratio of $M=2.0$. At blowing ratios greater than $M=2.0$, the 1.2*D* trench resulted in higher effectiveness levels than seen at the low blowing ratios.

Contrary to trenches, the bumps at heights of 0.5*D* and 0.8*D* showed very little effect on adiabatic effectiveness levels. Bumps of height 1.2*D* showed higher enhancements at lower blowing ratios and the enhancement levels dropped with an increase in blowing ratio beyond $M=1.0$. The maximum enhancement shown by the 1.2*D* bump was about 20%. From the baseline study, it was

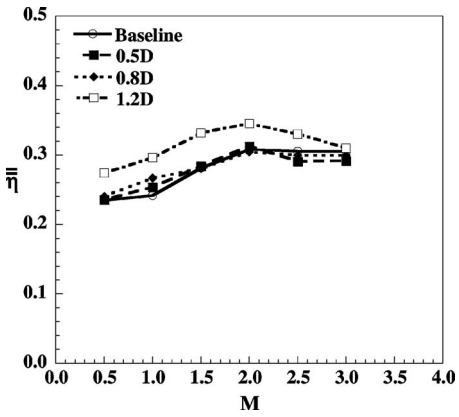

Fig. 14 Area-averaged effectiveness showing the effect of varying bump heights

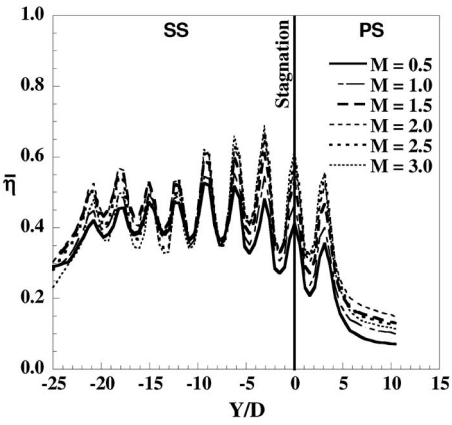

Fig. 16 Laterally averaged effectiveness showing the effect of the 1.2*D* bump at different blowing ratios

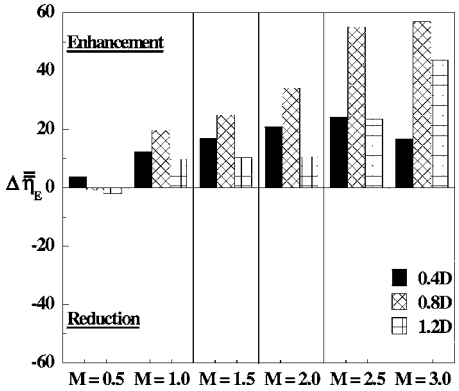

Fig. 17 Comparison of percent enhancement on area-averaged adiabatic effectiveness as a result of placing trenches at the leading edge

seen that without any modification at the leading edge, the maximum effectiveness was achieved at a blowing ratio of $M=2.0$. As bumps and trenches both showed an enhancement, it is important to see if these modifications at lower blowing ratios can show any enhancement when directly compared to the baseline case of $M=2.0$. This is important as it will ascertain if it will require less coolant, which in turn will increase the efficiency of the engine.

Figure 19 compares the enhancements resulting from the $0.8D$ trench and $1.2D$ bump relative to a baseline case of effectiveness achieved at $M=2.0$. The $0.8D$ trench and $1.2D$ bump were chosen as these were found to show the maximum enhancement for a particular geometry. For both the trenches and bumps, enhancements were only measured for $1.5 \leqslant M \leqslant 2.5$ and beyond $M=2.5$, only trenches were measured to have a positive augmentation. Even in this comparison, as previously discussed, the trenches performed better than the bumps. It needs to be seen whether a reduction in blowing ratio to $M=1.5$, showing an enhancement of only 10–15%, is more favorable than operating at the same blowing ratio of $M=2.0$ to achieve an enhancement of 35% (trenches).

Conclusions

Measurements of adiabatic effectiveness levels were presented at the leading edge-endwall junction where cooling is made difficult by the presence of a horseshoe vortex. In an attempt to improve cooling performance from a row of film-cooling holes placed near the junction, incorporating bumps and trenches were evaluated.

Trenches were applied in two different configurations. Individual hole trenches and row trenches were evaluated for a range

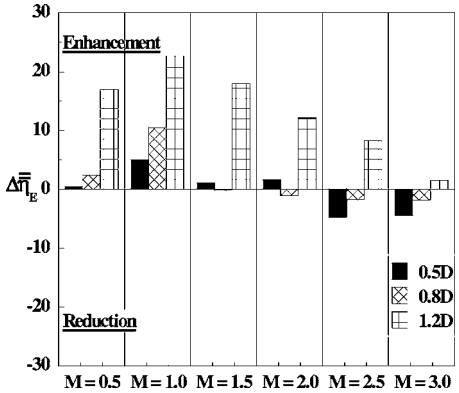

Fig. 18 Comparison of percent enhancement on area-averaged adiabatic effectiveness as a result of placing bumps at the leading edge

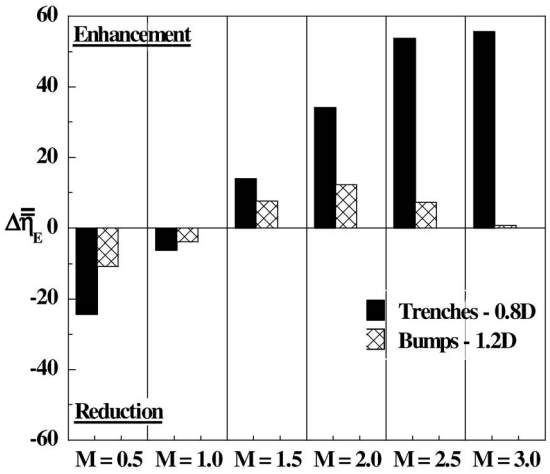

Fig. 19 Comparison of percent enhancement on area-averaged adiabatic effectiveness on trenches and bumps when compared to the baseline case at $M=2.0$

of blowing ratios and trench depths. Individual hole trenches showed very little effect on adiabatic effectiveness levels, whereas the row trenches showed a considerable enhancement. The $0.8D$ trench depth was found to be an optimum relative to the three depths studied at different blowing ratios. It was also found that the success of the trench on improving effectiveness levels is highly sensitive to blowing ratio for a particular trench depth.

Bumps with heights of $0.5D$ and $0.8D$ did not produce a major effect on effectiveness, although a bump height of $1.2D$ did show an enhancement of approximately 20% at a blowing ratio of $M=1.0$. Overall, this study has shown that it is possible to achieve improved film cooling at the vane-endwall junction through the use of small surface modifications near the cooling hole exits.

Acknowledgment

This publication was prepared with the support of the US Department of Energy, Office of Fossil Fuel, and National Energy Technology Laboratory. The authors thank Mike Blair (Pratt & Whitney), Ron Bunker (General Electric), and John Weaver (Rolls-Royce) for their input on the modeling of realistic turbine features.

Nomenclature

C = true chord of stator vane
D = diameter of film-cooling hole
h = height/depth of trenches and bumps
M = blowing ratio based on inlet mainstream velocity $M=\rho_j U_j/\rho_\infty U_\infty$
P = vane pitch; hole pitch
PS = pressure side
Re_{in} = Reynolds number defined as $\mathrm{Re}_{in}=CU_{in}/\nu$
S = span of stator vane; total vane surface length
SS = suction side
T = temperature
x = length along the vane surface
X,Y,Z = local coordinates
U = velocity

Greek

η = adiabatic effectiveness, $\eta=(T_\infty-T_{aw})/(T_\infty-T_c)$
$\bar{\eta}$ = laterally averaged effectiveness
$\bar{\bar{\eta}}$ = area-averaged effectiveness
$\Delta\bar{\bar{\eta}}_E$ = percent reduction in area-averaged effectiveness, $\Delta\bar{\bar{\eta}}_E=[(\bar{\bar{\eta}}_{\text{effect}}-\bar{\bar{\eta}}_{\text{base line}})/\bar{\bar{\eta}}_{\text{base line}}]\times 100$
ν = kinematic viscosity

Subscripts

aw = adiabatic wall
c = coolant conditions
in = inlet conditions
j = coolant flow through film-cooling holes
∞ = local freestream conditions
E = enhancement

References

[1] Chyu, M. K., 2001, "Heat Transfer Near Turbine Nozzle Endwall," Ann. N.Y. Acad. Sci., **934**, pp. 27–36.
[2] Friedrichs, S., Hodson, H. P., and Daws, W. N., 1996, "Distribution of Film-Cooling Effectiveness on a Turbine Endwall Measured Using Ammonia and Diazo Technique," ASME J. Turbomach., **118**, pp. 613–621.
[3] Friedrichs, S., Hodson, H. P., and Dawes, W. N., 1997, "Aerodynamic Aspects of Endwall Film-Cooling," ASME J. Turbomach., **119**, pp. 786–793.
[4] Friedrichs, S., Hodson, H. P., and Dawes, W. N., 1999, "The Design of an Improved Endwall Film-Cooling Configuration," ASME J. Turbomach., **121**, pp. 772–780.
[5] Thole, K. A., and Knost, D. G., 2005, "Heat Transfer and Film-Cooling for the Endwall of a First Stage Turbine Vane," Int. J. Heat Mass Transfer, **48**, pp. 5255–5269.
[6] Blair, M. F., 1974, "An Experimental Study of Heat Transfer and Film-Cooling on Large-Scale Turbine Endwalls," ASME J. Heat Transfer, **96**, pp. 524–529.
[7] Knost, D. G., and Thole, K. A., 2005, "Adiabatic Effectiveness Measurements of Endwall Film-Cooling for a First Stage Vane," ASME J. Turbomach., **127**, pp. 297–305.
[8] Cardwell, N. D., Sundaram, N., and Thole, K. A., 2007, "The Effects of Varying the Combustor-Turbine Gap," ASME J. Turbomach., **129**, pp. 756–764.
[9] Burd, S. W., and Simon, T. W., 2000, "Effects of Slot Bleed Injection Over a Contoured Endwall on Nozzle Guide Vane Cooling Performance—Part II: Thermal Measurements," ASME Paper No. 2000-GT-0200.
[10] Bunker, R. S., 2002, "Film-Cooling Effectiveness Due to Discrete Holes Within a Transverse Surface Slot," ASME Paper No. GT2002-30178.
[11] Lu, Y., Nasir, H., and Ekkad, S. V., 2005, "Film-Cooling From a Row of Holes Embedded in Transverse Slots," ASME Paper No. GT2005-68598.
[12] Waye, S. K., and Bogard., D. G., 2007, "High Resolution Film-Cooling Effectiveness Measurements of Axial Holes Embedded in a Transverse Trench With Various Trench Configurations," ASME J. Turbomach., **129**, pp. 294–302.
[13] Sundaram, N., and Thole, K. A., 2007, "Effects of Surface Deposition, Hole Blockage, and Thermal Barrier Coating Spallation on Vane Endwall Film Cooling," ASME J. Turbomach., **129**, pp. 599–607.
[14] Bunker, R. S., 2001, "A Method for Improving the Cooling Effectiveness of a Gaseous Coolant Stream," U.S. Patent No. 6,234,755.
[15] Radomsky, R., and Thole, K. A., 2002, "Flowfield Measurements for a Highly Turbulent Flow in a Stator Vane Passage," ASME J. Turbomach., **122**, pp. 255–262.
[16] Ethridge, M. I., Cutbirth, J. M., and Bogard, D. G., 2000, "Scaling of Performance for Varying Density Ratio Coolants on an Airfoil With Strong Curvature and Pressure Gradient Effects," ASME J. Turbomach., **123**, pp. 231–237.
[17] Moffat, R. J., 1988, "Describing the Uncertainties in Experimental Results," Exp. Therm. Fluid Sci., **1**, pp. 3–17.